Accelerated phosphorus removal using sulfate-coated expanded vermiculite

Taeyoon Lee[1]

[1]*Faculty of Environmental Engineering, Pukyong National University, Busan, Korea*

This study evaluated whether phosphorus in an aqueous solution can be effectively adsorbed and removed by sulfuric acid (SA)-coated vermiculite (SCV), which was synthetized by heating a mixture of expanded vermiculite (EV) and SA at 300°C. Phosphorus was removed from the aqueous solution and removal characteristics were evaluated by batch kinetic, batch adsorption, and column tests. The phosphate removal rates (h^{-1}) for 1, 2.5, 5, 7.5, 12.5, and 25 $g \cdot L^{-1}$ of SCV were 0.00015, 0.0011, 0.0044, 0.0087, 0.0648, and 0.5002, respectively. The Q_{max} of the Langmuir model and the partition coefficients of the linear and Freundlich models were 8.92 $mg \cdot g^{-1}$, 0.65 $L \cdot g^{-1}$, and 4.60 $L \cdot g^{-1}$ ($1/n = 0.354$), respectively. The equilibrium phosphorus adsorptions (q_e) were 7.47, 14.69, and 19.53 $mg \cdot g^{-1}$ at initial concentrations of 10, 25, and 50 $mg \cdot L^{-1}$, respectively. These results show that SCV can efficiently adsorb phosphorus in an aqueous solution.

INTRODUCTION

Domestic sewage, industrial wastewater, fertilizers, and livestock excretions lead to excessive accumulation of nutrient salts in drainage basins that can lead to eutrophication, deteriorating water quality, and other negative environmental effects (De-Bashan and Bashan, 2004; Song et al., 2007; Guan et al., 2009; Saha et al., 2008; Awual and Jyo, 2011; Huang et al., 2015). Eutrophication promotes abnormal growth of phytoplankton such as algae and eventually leads to death of fish and other aquatic organisms by exhausting dissolved oxygen (Estrada et al., 2011; Yang et al., 2013; Cabrita et al., 2015; Lapointe et al., 2015; Tekile et al., 2015). Water may smell foul when vegetation and algae decompose, and its turbidity also increases (Estrada et al., 2011; Yang et al., 2013). The eutrophication process can produce environmental toxins such as microcystins that can be ingested by humans (Codd et al., 2005; Yuan et al., 2006; Dittmann and Wiegand, 2006).

Excessive nutrients, such as nitrogen and phosphorus, must be removed from lakes and rivers to prevent eutrophication; however, the phosphorus usually occurs in aqueous form with limited sources and a relatively low influx compared to nitrogen. Thus, it is termed a limiting nutrient source and its removal is the most efficient way of preventing eutrophication in lakes and rivers (Zeng et al., 2004; Biswas et al., 2007; Kim et al., 2008; Lurling and Oosterhout, 2013; Lurling et al., 2014; Ogata et al., 2015). Phosphorus can be eliminated by physical, chemical, and biological methods. Current physical methods are microfiltration (Lu and Liu, 2010), reverse osmosis (Kartashevsky et al., 2015), and electrodialysis; chemical methods include precipitation, crystallization (Oladoja et al., 2013), cation exchange (Ruixia et al., 2002), and adsorption (Yang et al., 2013; Karaca et al., 2004; Choi et al., 2012); and biological methods are anaerobic-aerobic-activated sludge processing and enhanced biological phosphorus removal (Munch and Barr, 2001; Vaiopoulou and Melidis, 2007). The physical methods are generally easy and stable but costly (Nguyen et al., 2014). Electrodialysis and reverse osmosis have low efficiency, with removal of just 10% of total phosphorus (Karaca et al., 2004). Precipitation produces additional sludge that creates treatment and disposal issues and has high chemical treatment costs (De-Bashan and Bashan, 2004; Ruixia et al., 2002; Kumar et al., 2010; Zhang et al., 2011). The biological methods also have disadvantages. They are dependent on favourable microbial environmental conditions and require considerable space to complete treatment, making it difficult to implement continuous and stable treatments (Nguyen et al., 2014; Jung et al., 2000; Ning et al., 2008).

The adsorption method is convenient in comparison to the physical, chemical, and biological methods. It is economical, with a high selectivity for phosphorus that can increase removal rates at lower costs (Yang et al., 2013; Karaca et al., 2004; Zhang et al., 2011); furthermore, because it is possible to apply adsorption to water of varying quality, it can be widely applied. A variety of low-cost adsorbents for the removal of phosphorus have been developed using industrial by-products such as red mud (Akay et al., 1998), dolomite (Karaca et al., 2004), fly ash (Guan et al., 2009; Cheung and Venkitachalam, 2000; Wen et al., 2014), olivine (Lee and Yim, 2011), steel slag (Bowden et al., 2009), and zirconium (Biswas et al., 2008).

The vermiculite used in this study is a clay mineral composed of magnesium, iron, and aluminium, with a 2:1 combination structure between tetrahedral-silica and octahedral-alumina sheets. The mineral has a high cation exchange ratio of 120–150 $meq \cdot 100 \, g^{-1}$ from the ion exchange between the surface and internal areas, and heating of 800~1,100°C results in expansion of about 6–20 times, turning it into a porous media with a large specific surface area that allows it to float on water (Malandrino et al., 2006; Song et al., 2009). In addition, because vermiculite is abundant and low-cost, it can be applied as a filter adsorbent on roads during rainstorms or be used as a natural adsorbent (Kim and Lee, 2014).

CORRESPONDENCE
Taeyoon Lee

EMAIL
badger74w@pknu.ac.kr

DATES
Received: 18 February 2019
Accepted: 14 August 2020

KEYWORDS
vermiculite
sulfuric acid
floating adsorbent
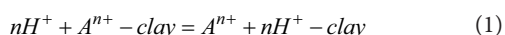adsorption
exfoliation
phosphorus

WATER SA

Many heterogeneous catalysis adsorbents have been made based on vermiculite for removal of various water pollutants, such as chitosan/vermiculite biocomposite (Chen et al., 2017), amphoteric modified vermiculite (Liu et al., 2017), amphoteric surfactant activated montmorillonite (Liu et al., 2016), and peroxymonosulfate activated with Fe⁰-montmorillonite (Yang et al., 2018).
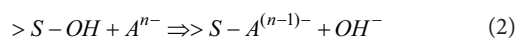
Because all surface-coating adsorbent methods are not equally efficient in removing phosphorus, research continues to explore methods to increase sorption efficiency. Choi et al. (2012) reported the use of zeolite and activated alumina coated by sulfuric acid (SA); however, to our knowledge, no study has been done on the use of SA-coated vermiculite (SCV) for the removal of phosphorus. Anionization of adsorbents using sulfuric acid enables adsorbents to have a negative charge by combining sulfate ions with adsorbents. Common chemicals used for the anionization are $(NH_4)_2SO_4$ and H_2SO_4.

In general, cations such as Ca^{2+}, Mg^{2+}, Al^{3+}, Fe^{3+}, K^+, Na^+ included in clay-type adsorbents leach from tetrahedral and octahedral layers when the adsorbents react with sulfuric acid, and H^+ ions substitute for leached cations (Del Gastillo and Grange, 1997). From this reaction, acidity of clay-type adsorbents increases. This reaction is expressed as follows.

$$nH^+ + A^{n+} - clay = A^{n+} + nH^+ - clay \tag{1}$$

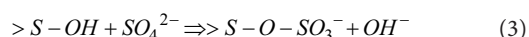where A indicates cations in clay-type adsorbents.

Combination of adsorbents and anions in water easily occurs in clay-type adsorbents (for example, vermiculite) containing hydroxide (OH^-) ions. The reaction of a combination of clay-type adsorbents and anions is represented as follows (McBride, 1994):

$$> S - OH + A^{n-} \Rightarrow > S - A^{(n-1)-} + OH^- \tag{2}$$

where A^{n-} is anion in water and >S-OH represents a metal hydroxyl group.

This ligand exchange reaction occurs effectively at low pH. Thus, the activity of clay-type adsorbents should be lower according to Eq. 1.

When sulfuric acid is used with the clay-type adsorbents to promote the ligand exchange reaction, the reaction is expressed as follows (McBride, 1994):

$$> S - OH + SO_4^{2-} \Rightarrow > S - O - SO_3^- + OH^- \tag{3}$$

Cations in clay-type adsorbents are replaced by H^+ ions and SO_4^{2-} is bonded to the clay-type adsorbents in the form of SO_3^-.

Anion exchange of SO_3^- in clay-type adsorbents with phosphorus in water occurs according to differences in shared charge among SO_3^- or phosphorus with metal hydroxyl groups. In general, lower shared charge indicates higher binding force with anion and metal hydroxyl groups. Clay-type adsorbents containing SO_3^- show greater shared charge on metal hydroxyl groups than that of PO_4^{3-} on metal hydroxyl groups. Thus, SO_3^- in the adsorbents can be easily replaced by PO_4^{3-} in wastewater (McBride, 1994).

Here we report the results of surface characteristics of SCV and results of phosphorus removal by SCV. Elemental scanning electron microscopy and energy dispersive x-ray spectroscopy (SEM-EDS), x-ray fluorescence (XRF), x-ray powder diffraction (XRD), and Fourier transform infrared spectroscopy (FTIR) analyses were performed to evaluate the surface characteristics of SCV, and the adsorption capacity of SCV for phosphorus was determined using batch kinetic, batch sorption, and flow-through column tests.

MATERIALS AND METHODS

Materials

Vermiculite expanded about 15 times (Samhwa, Kwangjoo, Korea) was washed with DI water, and then stored in a desiccator until use. Vermiculite particles less than 3 mm diameter were used.

H_2SO_4 (95% purity; Junsei Chemical, Japan) was used as the reagent for the SA coating. KH_2PO_4 (99% purity) was obtained from Junsei Chemical Corporation (Junsei, Japan). 0.439 g of KH_2PO_4 was dissolved in 1 L of DI water to make 100 mg·L⁻¹ PO_4^{3-}. The phosphorus solution was prepared by using 100 mg·L⁻¹ PO_4^{3-} for the phosphorus-adsorption experiment, and the concentration of phosphorus after reaction was measured by a DR900 Colorimeter (HACH, USA). A 0.45-μm Teflon syringe filter was used to filter all samples before measurement.

Production of adsorbents

Bulk dry density was determined using a DME-220HE tuning fork density meter (Shinko Denshi Co., Japan).

The SCV was synthetized by mixing 50 g of EV and 500 mL of 10% H_2SO_4 in a 1 L glass beaker as described by Choi et al. (2012). After reacting the mixture at room temperature for 12 h, the mixture was removed and heated in an electro-furnace (CT-DMF 1; Coretech, Korea) at 300°C for 3 h and then dried in an oven at 105°C. The drying matter was cleaned 5 times with distilled water until no further pH change was observed in DI water.

The quantities of C, H, N, and S in the EV and SCV were analysed by macro- and micro-elemental analysers (Elementar, Germany). Surface properties of EV and SCV were measured by SEM (S-2700; Hitachi, Japan). Oxide forms of EV and SCV were analysed by qualitative and quantitative analyses by XRF (XRF-1700; Shimadzu Scientific Instruments, Japan) and XRD (X'Pert-MPD System; Philips, Netherlands) was used to observe the crystal structure of the SCV. The spectra according to the molecular structure and molecular binding of the compounds were analysed using FTIR (Spectrum X; Perkin Elmer, USA).

Batch kinetic tests

Batch kinetic tests were performed to evaluate the removal rate of phosphorus in the presence of varying doses of adsorbents under different initial phosphorus concentrations. Designated doses of adsorbents were placed in 50-mL Teflon bottles filled with phosphorus solution (40 mL). The bottles were loaded on a shaker and rotated at 30 r·min⁻¹. Bottles were removed from the shaker intermittently for analysis. The sample was filtered through a 0.45-um Teflon syringe filter and prepared for analysis.

A first-order decay model with instantaneous adsorption was used to determine the bulk reaction rate constant (K_{obs}) and the instantaneous partition coefficient (K_p) for phosphorus. The model is (Koppensteiner, 1998):

$$C_{aq} = \frac{C_o}{1 + \frac{m}{v}K_p} \exp\left(\frac{-K_{obs} \cdot t}{1 + \frac{m}{v}K_p}\right) \tag{4}$$

where C_{aq} represents the phosphorus concentration (mg·L⁻¹) at a specific time, C_o is the initial phosphorus concentration (mg·L⁻¹), m is the mass of sorbent (g), v is the volume of phosphorus solution (mL), K_p (L·kg⁻¹) is the instantaneous partition coefficient for phosphorus and K_{obs} is a bulk first-order reaction rate constant (h⁻¹). Equation 1 was fitted to the data using a least-squares algorithm.

The data obtained from the batch kinetic tests were analysed using the pseudo first-order and second-order kinetic models.

The pseudo first-order kinetic model provided is expressed as Eq. 5.

$$\log(q_e - q_t) = \log q_e - k_1 t \qquad (5)$$

where q_e (mg·g⁻¹) and q_t (mg·g⁻¹) are the phosphate adsorbed amount at equilibrium and time t, respectively, and k_1 is the rate constant for the pseudo first-order kinetic model (min⁻¹). The pseudo second-order kinetic model is expressed as Eq. 6.

$$\frac{t}{q_t} = \frac{1}{k_2 q_e^2} + \frac{t}{q_e} \qquad (6)$$

where k_2 is the rate constant for the pseudo second-order kinetic model (g·mg⁻¹·min⁻¹). The values of k_2 and q_e are calculated from a plot of (t/q_t) versus t.

Batch adsorption tests

For the batch adsorption tests, the amount of adsorbent was maintained at a constant (0.2 g) while the initial concentration of phosphorus was varied from 10 to 50 mg·L⁻¹. Solution pHs for the batch and column tests were adjusted to 7.8 using NaOH and all the tests were performed at 23°C. Phosphorus solutions (40 mL) and adsorbent were placed into 50-mL bottles. The bottles were shaken at 30 r·min⁻¹ for 6 h. After tumbling, the bottles were centrifuged at 8 000 r·min⁻¹ (8 200 g) for 20 min. Samples were obtained from the bottles using a 5-mL gas-tight syringe, and then prepared for analysis as described previously.

A simple isothermal equation (i.e., those of the linear, Freundlich, and Langmuir isotherm models) was used to generate an adsorption isotherm to indicate the adsorption equilibrium of a single ingredient. Adsorption parameters for phosphorus were obtained by fitting linear (Eq. 7), Freundlich (Eq. 8), and Langmuir models (Eq. 9) to the data using a least-squares algorithm. These models are as follows:

$$C_s = K_p C_e \qquad (7)$$

$$C_s = K_f C_e^{1/n} \qquad (8)$$

$$C_s = \frac{Q_{max} K_l C_e}{1 + K_l C_e} \qquad (9)$$

where C_s is the concentration (mg·g⁻¹) of phosphorus that was adsorbed on the adsorbent, C_e is the equilibrium phosphorus concentration (mg·L⁻¹), K_p is the distribution coefficient of the linear model, and K_f (L·g⁻¹), $1/n$ are the Freundlich partition coefficient and adsorption constants related to the adsorption capacity and the intensity of adsorption, respectively. Q_{max} represents the maximum adsorption capacity (mg·g⁻¹), and K_l is a Langmuir adsorption constant related to the binding strength.

Leaching of SO₄²⁻ from SCV

Additional batch kinetic tests were performed to determine leaching characteristics of SO₄²⁻ from SCV during phosphorus removal tests. The tests were performed under conditions of SCV 25 g·L⁻¹ and initial phosphorus concentrations of 40 mg·L⁻¹. During the first tests, SO₄²⁻ and phosphorus were measured at designated sampling times. After the first test, SCV was filtered and dried at 80°C in a drying oven for 12 h. Then, the SCV was used for the second test under the condition of SCV 25 g·L⁻¹ and initial phosphorus concentration of 40 mg·L⁻¹ SO₄²⁻ and phosphorus were also measured at designated sampling times. The third experiment was conducted in the same way as the second experiment.

Column tests

Column tests were conducted to determine sorbent efficiency of phosphorus in flow-through conditions. A schematic of the column test setup is shown in Fig. 1. A glass column (length = 300 mm, diameter = 55 mm) was used with Teflon adapters and porous
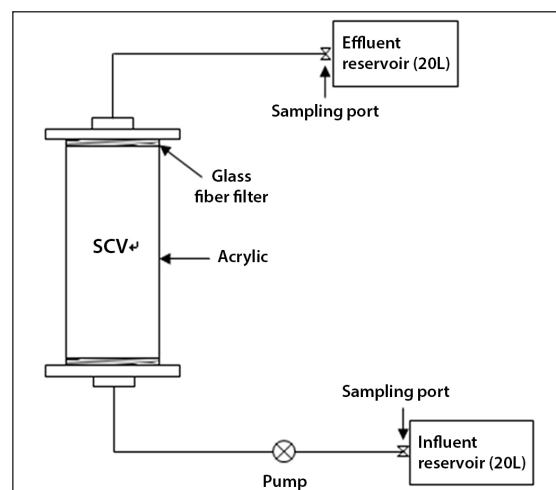

Figure 1. Schematic diagram of upward flow column test set-up

ceramic disks attached to both ends. 79.1 g of SCV was packed in the column (porosity = 0.42). Prior to the start of the experiment, 200 mL of DI water was added to the column to saturate the inside of the column with DI water. The influent solution was then switched to a phosphorus solution for the column test.

Solution was introduced into the column at a constant flow rate using a peristaltic pump (model BT100-1F; LongerPump, USA). All tests were conducted with upward flow. Concentrations of phosphorus in the influent were set as 10, 25, and 50 mg·L⁻¹.

The adsorbed phosphorus quantity in the column (q_{total}, mg) can be expressed by Eq. 10, as follows:

$$q_{total} = \frac{Q}{1000} \int_{t=0}^{t=total} C_a d_t \qquad (10)$$

where C_a represents the adsorbed phosphorus concentration (mg·L⁻¹), which is calculated by $C_o - C_t$ and Q is the inflow flow rate (mL·min⁻¹); in addition, the equilibrium adsorbed quantity q_e (mg·g⁻¹) is shown in Eq. 11, as follows:

$$q_e = \frac{q_{total}}{m} \qquad (11)$$

where m represents the mass of vermiculite (g) loaded in the column, and C_o, C_t is the initial concentration and concentration measured at time t.

Empty bed contact time (EBCT) of column tests is calculated as follows:

$$\text{EBCT (min)} = \text{bed volume (mL)} / \text{flowrate (mL·min}^{-1}) \qquad (12)$$

RESULTS AND DISCUSSION

Elemental analysis of adsorbents

The dry density of the EV was 0.25 g·cm⁻³ and a similar dry density was obtained for SCV (0.26 g·cm⁻³). The values of the elemental analysis for the EV and SCV are summarized in Table 1. The C and N concentrations of both the EV and SCV were similar: 0.22% and 0.20% (C) and 0.49% and 0.79% (N), for EV and SCV, respectively; however, the concentrations of H and S were considerably different. H concentrations of EV and SCV were 0.75% and 1.29%, and those of S were 0.28% and 5.68%, respectively. The large difference in the H and S concentrations could be related to the addition of sulfate (SO₄²⁻) during coating.

Table 1. Elementary analysis of EV and SCV

Adsorbent	Elemental analyses (wt, %)			
	C	H	N	S
EV	0.22	0.752	0.49	0.281
SCV	0.20	1.289	0.79	5.683

Table 2. Chemical compositions of EV and SCV determined by x-ray fluorescence

Adsorbent	SiO_2	Al_2O_3	MgO	Fe_2O_3	CaO	K_2O	TiO_2	SO_3	Na_2O	Cr_2O_3	NiO
EV	44.41	12.49	27.2	4.96	1.38	5.96	1.44	0.08	1.29	0.38	0.06
SCV	43.14	8.92	18.85	4.01	0.48	5.46	1.52	16.87	0.37	0.31	0.04

XRF and XRD analyses of adsorbents

Table 2 indicates the XRF results for EV and SCV. EV mainly consisted of SiO_2, MgO, and Al_2O_3 (44.4%, 27.2%, and 12.5%, respectively). The percentages of SiO_2 and K_2O (43.14% and 5.46%) in SCV were similar for EV. SCV consisted of 18.9% MgO, 8.9% Al_2O_3, and 4.0% Fe_2O_3. All percentages of oxides in SCV decreased, with the exception of SO_3, which increased to 16.9%.

These results mean that the K^+ ion was not affected by the ion exchange of other metal cations or the metal complex, even with

the SA coating on EV, and that the K^+ ion in EV was not involved in the ion exchange due to the primary involvement of the biotite layer (Muiambo et al., 2015). In addition, the quantity of CaO in EV and SCV decreased from 1.38% to 0.48%, which can be explained by the substitution of the considerable quantity of Ca^{2+} ions between the vermiculite layers with H^+.

Figure 2 shows results of the XRD analysis. EV had the highest peaks at 2θ (8.01°, 28.09°, and 44.93°), as did SCV (9.03° and 26.61°); the EV 8.01° peak represents a mica impurity in the vermiculite and the 44.93° peak is caused by aluminium (Medeiros et al., 2009; Sousa et al., 2012). From Fig. 2, it is assumed the crystallization was weakened by the greater decrease of the SCV reflection intensity compared with that of EV, but its original structure was not greatly changed.

SEM-EDS analysis of adsorbents

Figure 3 shows the SEM images for EV and SCV. In Fig. 3a, the smooth EV surface appears as a laminated structure with an accordion-like layer. The SCV surface is shown in Fig. 3b, and a modification between the surface and a vermiculite layer from heating to a high temperature is evident. Figure 3c shows the surface of SCV after adsorption tests are performed. In the case of EV, the surface was smooth, but in the case of SCV, it was confirmed that many cracks were formed on the surface. Since many particles were formed on the surface of the SCV after the adsorption experiment, it is judged to be a change due to the adsorption of phosphorus.
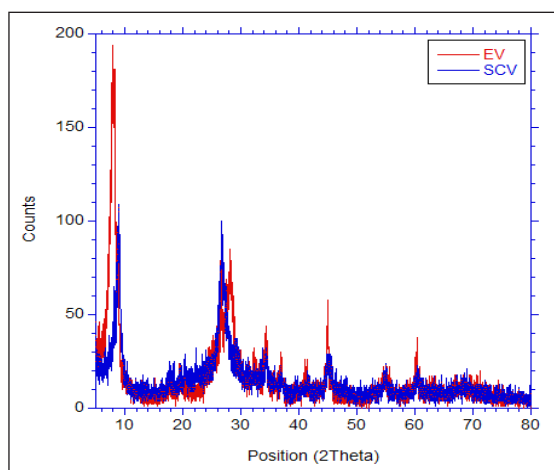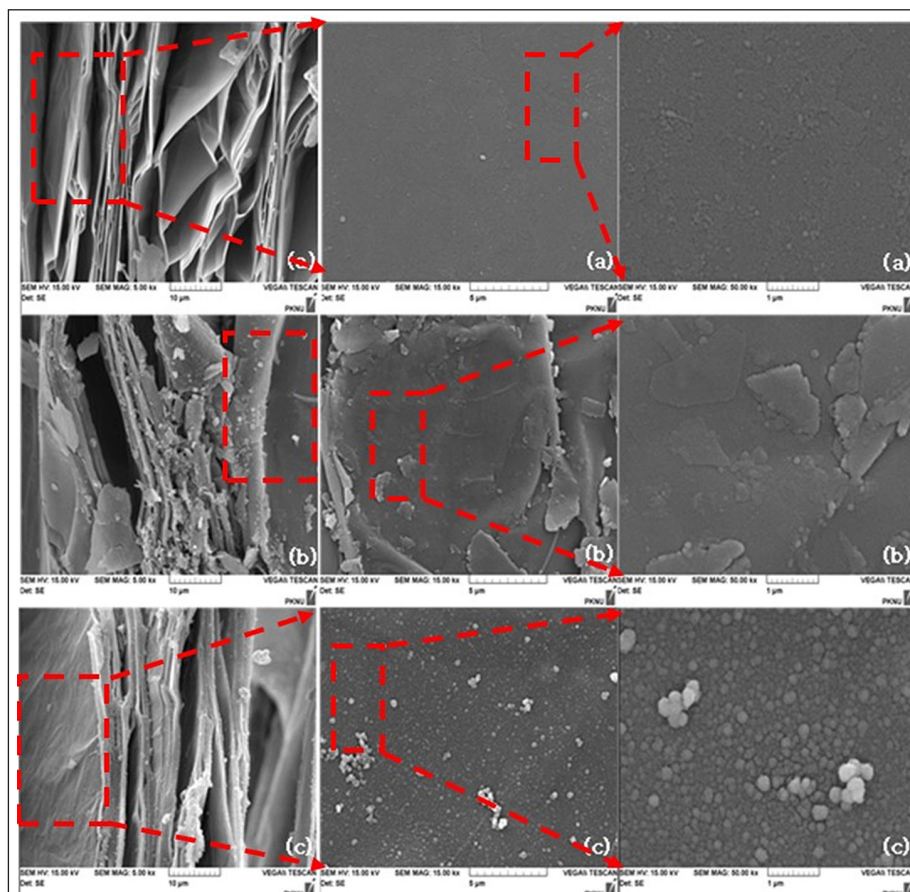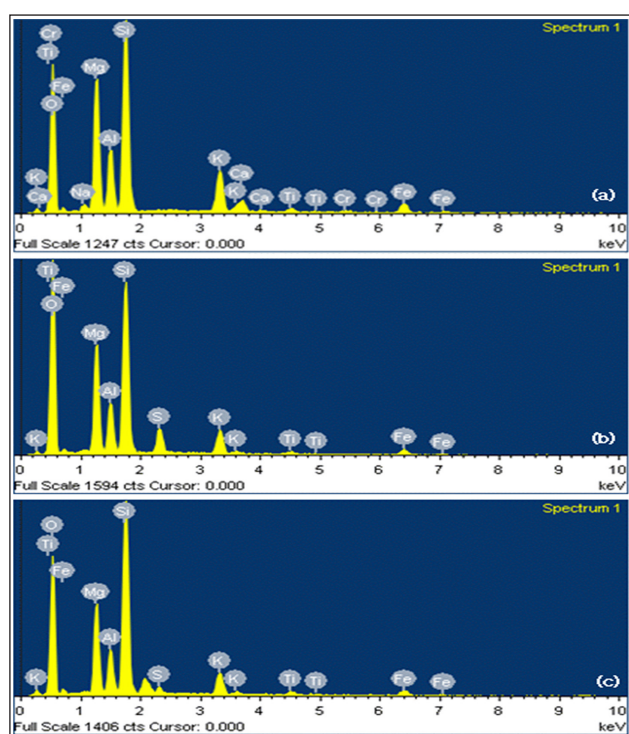

Figure 2. XRD pattern of EV and SCV

Figure 3. SEM images of (a) EV, (b) SCV, and (c) SCV after batch sorption tests

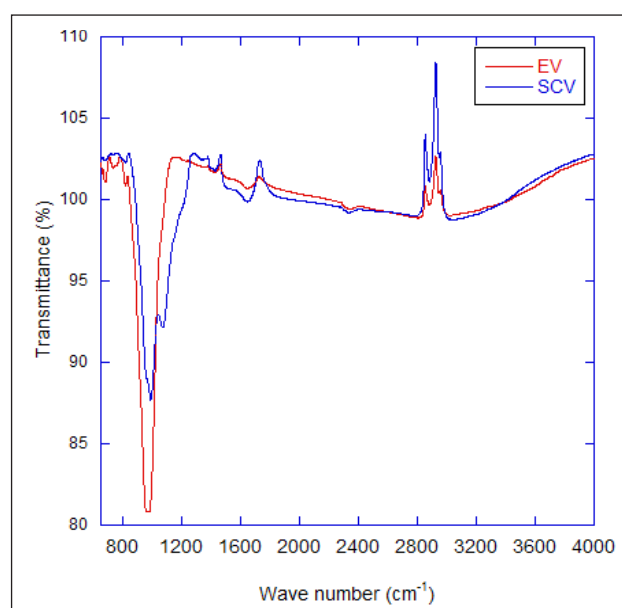**Table 3.** EDS analysis of EV, SCV and SCV after phosphorus adsorption

Elements	EV		SCV		After adsorption	
	Mass ratio (wt.%)	Atomic ratio (at.%)	Mass ratio (wt.%)	Atomic ratio (at.%)	Mass ratio (wt.%)	Atomic ratio (at.%)
O	48.8	63.3	56.89	70.1	52.4	66.32
Na	0.85	0.77	0	0	0	0
Mg	13.71	11.7	11.32	9.18	11.1	9.24
Al	6.1	4.69	4.94	3.61	4.69	3.52
Si	19.27	14.24	18.1	12.7	23.7	17.09
K	5.32	2.82	3.21	1.62	3.67	1.9
Ca	1.43	0.74	0	0	0	0
Ti	0.79	0.34	0.46	0.19	0.81	0.34
Cr	0.3	0.12	0	0	0	0
Fe	3.43	1.27	2.03	0.72	2.63	0.95
S	0	0	3.06	1.88	0.99	0.63

Figure 4. Results of EDS analysis of (a) EV, (b) SCV, and (c) SCV after batch sorption tests

The results of the dispersive x-ray spectroscopy (SEM-EDS) analysis are shown in Fig. 4 and summarized in Table 3. Here the S peak (3.06%) that could not exist in EV is observed in SCV, indicating that sulfate (SO_4^{2-}) is attached to the vermiculite after coating with SA. Because sulfate coated on SCV has a lower shared charge value than phosphorus in water, it is considered that the concentration is reduced because it is easily replaced by phosphorus. In addition, the Al, Mg and Fe peaks in the SCV are decreased more than those in EV. Like the XRF results, SEM-EDS shows that the octahedral cation was leached after the SA-coating treatment (Long et al., 2014).

FTIR analysis of adsorbents

Figure 5 shows the FTIR spectra of EV and SCV. The strongest peaks of EV and SCV are shown at 974 cm^{-1} and 989 cm^{-1}, respectively, representing the stretching vibrations of the Si-OH non-bridging oxygen atoms (Shin et al., 2004). EV peaks at 680 cm^{-1}, 735 cm^{-1} and 974 cm^{-1} are relevant to the Si-O stretching vibration between Si–O–Si in the silica layer and Si–OH in

Figure 5. Results of FTIR spectra of EV and SCV

the tetrahedral sheet, a structural property of the vermiculite (Long et al., 2014). This peak weakened after the SA coating, possibly because the octahedral cation was diminished due to the extraction from the octahedral sheet (Long et al., 2014). The 1 648 cm^{-1} peak is mainly due to the absorption of δ (H$_2$O) by a water molecule in the vermiculite, and explains why the silica layer changed from hydrophilic to hydrophobic (Long et al., 2014; Yu et al., 2010). Additionally, the attachment of sulfate in SCV is observed at the 1 067 cm^{-1} peak (Choi et al., 2012).

Batch kinetic tests

For the comparison of EV and SCV for the removal of phosphorus, one batch test was conducted for phosphorus removal. Figure 6 shows the concentrations of phosphorus removed by the EV and SCV where 0.5 g of adsorbent in 40 mL solution and initial phosphorus concentration of 20 mg·L^{-1} was used. Phosphorus concentrations were dramatically decreased within 10 s (more than 80%), but the EV, unlike the SCV, removed little phosphorus. The good correspondence between the data and the equation fit indicates that phosphorus removal follows a first-order reaction. The K_{obs} (h^{-1}) and K_p (L·kg^{-1}) of SCV were 0.377 and 684.8, respectively. On the contrary, no fitting parameters were obtained for EV. The K_{obs} (h^{-1}) and K_p (L·kg^{-1}) for the batch kinetic tests are summarized in Table 4.

Table 4. Instantaneous partition coefficients and first-order rate constants for phosphorus removal using various vermiculites under different test conditions

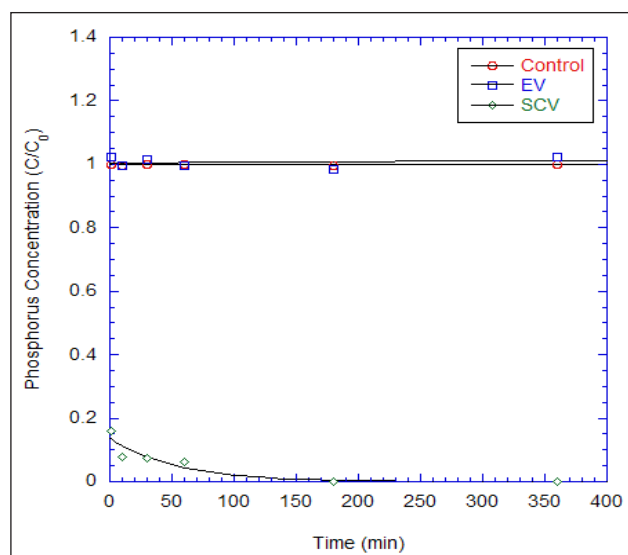| Reactive media	Dose (g·L⁻¹)	Initial phosphorus concentration (mg·L⁻¹)	Removal rate after 6 h (%)	K_{obs} (h⁻¹)	K_p (L·kg⁻¹)
EV	12.5	20	-	-	-
SCV	12.5	20	99.99	0.377	684.81
SCV	1	40	9.5	0.00015	58.97
SCV	2.5	40	35	0.0011	67.90
SCV	5	40	71.75	0.0044	78.83
SCV	7.5	40	85.25	0.0087	90.17
SCV	12.5	40	99.99	0.0648	141.07
SCV	25	40	99.99	0.5002	166.61
SCV	12.5	10	99.99	0.549	730.66
SCV	12.5	20	99.99	0.377	684.81
SCV	12.5	30	99.99	0.208	370.54
SCV	12.5	40	99.99	0.065	141.07
SCV	12.5	50	99.01	0.032	112.72

Figure 6. Adsorption of phosphorus by EV and SCV according to the time (adsorbent concentration: 25 g·L⁻¹; phosphorus concentration: 20 mg·L⁻¹)

On the basis of the above results, SCV was selected as an adsorbent for the removal of phosphorus, and additional batch kinetic tests were conducted for various ratios of an adsorbent–phosphorus solution. Phosphorus removal patterns for different ratios of SCV and phosphorus solution of 40 mL with an initial phosphorus concentration of 40 mg·L⁻¹ are shown in Fig. 7 and Table 4. The removal rates for 1, 2.5, 5 and 7.5 g·L⁻¹ of SCVs at a time of 360 min were 9.5%, 35%, 71.75% and 85.25%, respectively. As no phosphorus was detected after 60 min at 12.5 g·L⁻¹ and 25 g·L⁻¹ of SCVs, the removal rates were almost 99.99%. Based on these results, we can confirm that higher SCV dosage results in higher removal rates. The fitting parameters obtained by applying Eq. 4 to the phosphorus removal data are shown in Fig. 7b. The removal rate constant K_{obs} (h⁻¹) shows a rapidly increasing pattern as the amount of SCV increases: 0.00015 at 1.0 g·L⁻¹ to 0.5002 at 25 g·L⁻¹. Furthermore, the instantaneous partition coefficient K_p (L·kg⁻¹) was quickly increased, similarly to the removal rate constant, from 58.97 at 1 g·L⁻¹ to 166.61 at 25 g·L⁻¹.

Figure 8 shows the concentration changes of the phosphorus solutions with time, where the initial concentrations are 10, 20,
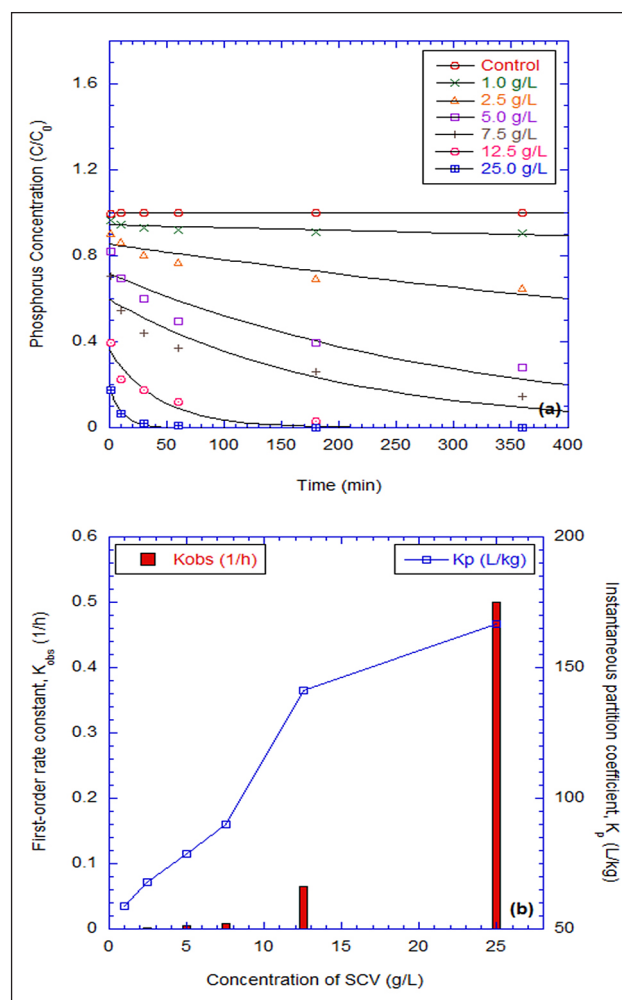

Figure 7. Adsorption behaviour of phosphorus at (a) different dosage of SCV and (b) fitting parameters obtained by Eq. 4

30, 40 and 50 mg·L⁻¹, and 0.5 g of SCV is added. Test conditions are summarized in Table 4. The phosphorus ions were effectively removed, with removal rates of almost 99%. With these results, the first-order rate constant and instantaneous partition coefficient were obtained using Eq. 4 and the results are summarized in Table 4.

Table 5. The pseudo first-order kinetic model and the pseudo second-order kinetic model parameter of phosphorus adsorption with different initial concentrations, using SCV

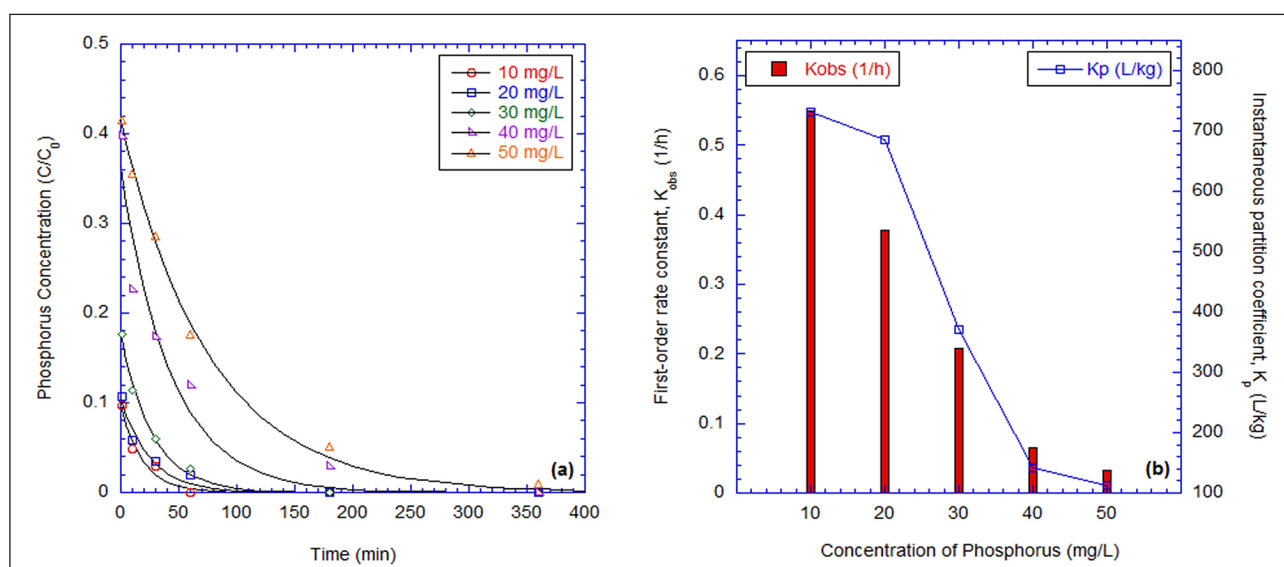| Initial conc. (mg·L⁻¹)	$q_{e.exp}$ (mg·g⁻¹)	Pseudo first-order kinetic model				Pseudo second-order kinetic model			
		$q_{e.cal}$ (mg·g⁻¹)	k_1 (min⁻¹)	R^2	Δq (%)	$q_{e.cal}$ (mg·g⁻¹)	k_2 (g·mg⁻¹·min⁻¹)	R^2	Δq (%)
10	0.8	0.044	0.0065	0.8049	55.51	0.801	3.064	1.0000	0.00072
20	1.6	0.114	0.0068	0.9288	54.13	1.604	0.833	1.0000	0.00085
30	2.4	0.292	0.0075	0.9298	45.78	2.409	0.332	1.0000	0.0025
40	3.2	1.061	0.0061	0.9667	22.73	3.227	0.063	0.9995	0.0173
50	3.96	1.568	0.0055	0.9956	15.17	4.021	0.031	0.9988	0.0136

Figure 8. Adsorption behaviour of phosphorus tested with 12.5 g·L⁻¹ SCV at (a) different initial phosphorus concentrations and (b) fitting parameters obtained by Eq. 4
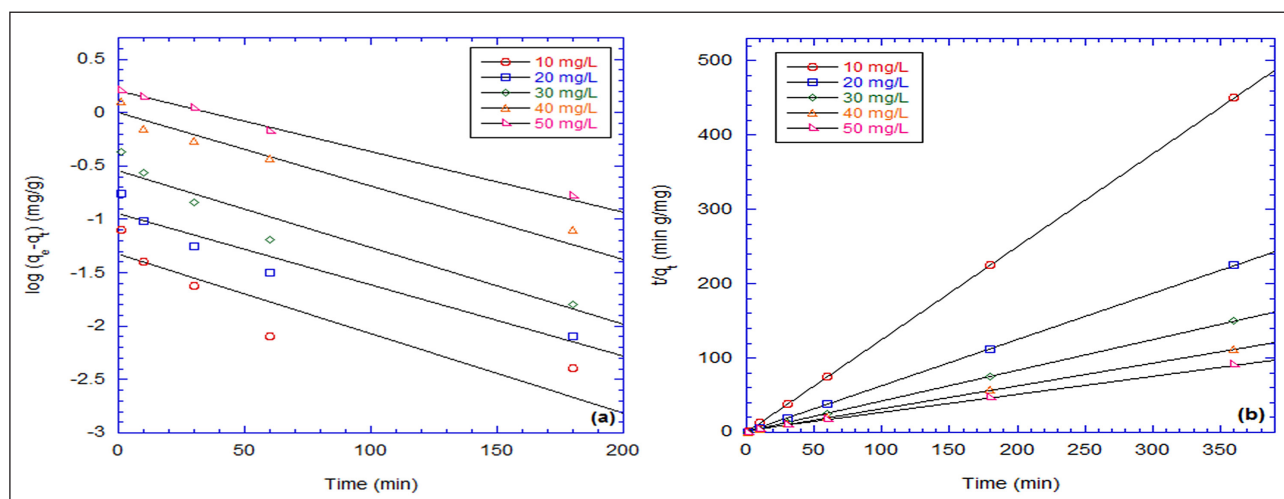

Figure 9. Results of (a) pseudo first-order model fits and (b) pseudo second-order model fitting for batch kinetic tests for different initial phosphorus concentrations (SCV concentration: 12.5 g·L⁻¹)

As shown in Fig. 8b, the highest concentration of phosphorus resulted in highest K_{obs} but lowest K_p. By increasing the initial concentration, the removal constants, K_{obs} (h⁻¹), were decreased to 0.549, 0.377, 0.208, 0.065 and 0.032. When the initial concentration was increased, the instantaneous partition coefficients decreased to 730.7, 684.8, 370.5, 141.1 and 112.7 L·kg⁻¹.

The parameters of pseudo first-order and second-order model are summarized in Table 5 and model fits are shown in Fig. 9. It is clear that the process of phosphate adsorption onto SCV is well described by the pseudo second-order model because of the
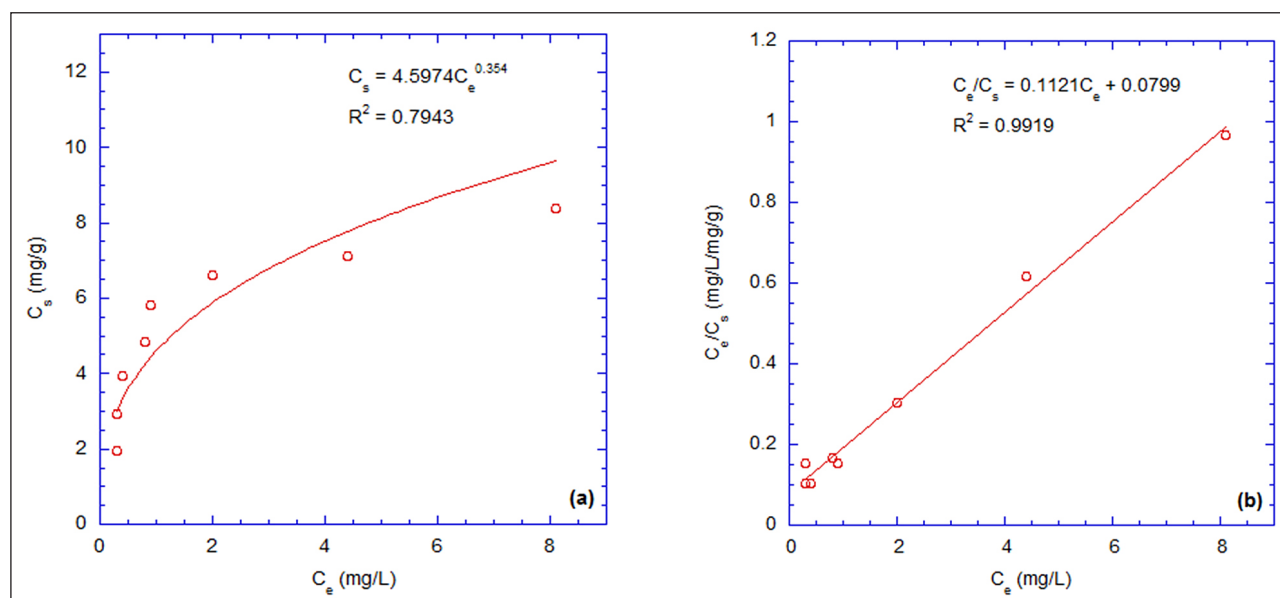
high correlation coefficient. The correlation coefficients for the fitting of the pseudo second-order model range between 0.9988 and 1.0000. The calculated amount of phosphate adsorbed on SCV at equilibrium ($q_{e,cal}$) was quickly increased from 0.80 mg·g⁻¹ at 10 mg·L⁻¹ to 4.02 mg·g⁻¹ at 50 mg·L⁻¹. This phenomenon was due to both increased contact time between adsorbent and adsorbate, and an increased concentration difference between the surface of the SCV and adsorbate in solution. On the contrary, k_2 (g·mg⁻¹·min⁻¹) was decreased from 3.064 at 10 mg·L⁻¹ to 0.031 at 50 mg·L⁻¹.

Table 6. Adsorption parameters of linear, Freundlich, and Langmuir models for phosphorus adsorption on the SCV

	Linear model		Freundlich model			Langmuir model		
	K_p (L·g^{-1})	R^2	K_f (L·g^{-1})	$1/n$	R^2	Q_{max} (mg·g^{-1})	K_l (L·mg^{-1})	R^2
SCV	0.6544	0.6845	4.5974	0.354	0.7943	8.921	1.403	0.9919

Table 7. Comparison of the maximum adsorption capacity of different adsorbents for phosphorus in aqueous solutions

Adsorbent	Removal capacity (mg·g^{-1})	Author
Kanuma mud	1.14	Yang et al. (2013)
Goethite	2.78	Zhong et al. (2007)
Lagoon fly ash	3.082	Cheung and Venkitachalam (2000)
Wood fibre	4.3	Eberhardt et al. (2006)
Alumina-coated carboxylated	5.23	Saha et al. (2008)
ACF-La	5.85	Zhang et al. (2011)
Lanthanum-doped vesuvianite	6.7	Li et al. (2009)
Iron oxide tailings	8.21	Zeng et al. (2004)
Sulfate-coated vermiculite	8.921	**In this study**
Zirconium ferrite	13	Biswas et al. (2008)
Scallop shell	23	Yeom and Jung (2008)
Activated red mud	23.23	Pradhan et al. (1998)
Sawdust	28.79	Unnithan et al. (2002)
Aluminium oxide	34.57	Peleka and Deliyanni (2009)
Hydrotalcite	60.00	Peleka and Deliyanni (2009)
Silica sulfate	46.32	Jutidamrongphan et al. (2012)
Hydrotalcite	22.22	Choi et al. (2012)
Activated alumina	49.67	Choi et al. (2012)
Zeolite	111.49	Choi et al. (2012)
nZVI	245.65	Wen et al. (2014)

Figure 10. Adsorption isotherms for phosphorus ions on SCV and model fit with (a) Freundlich and (b) Langmuir models
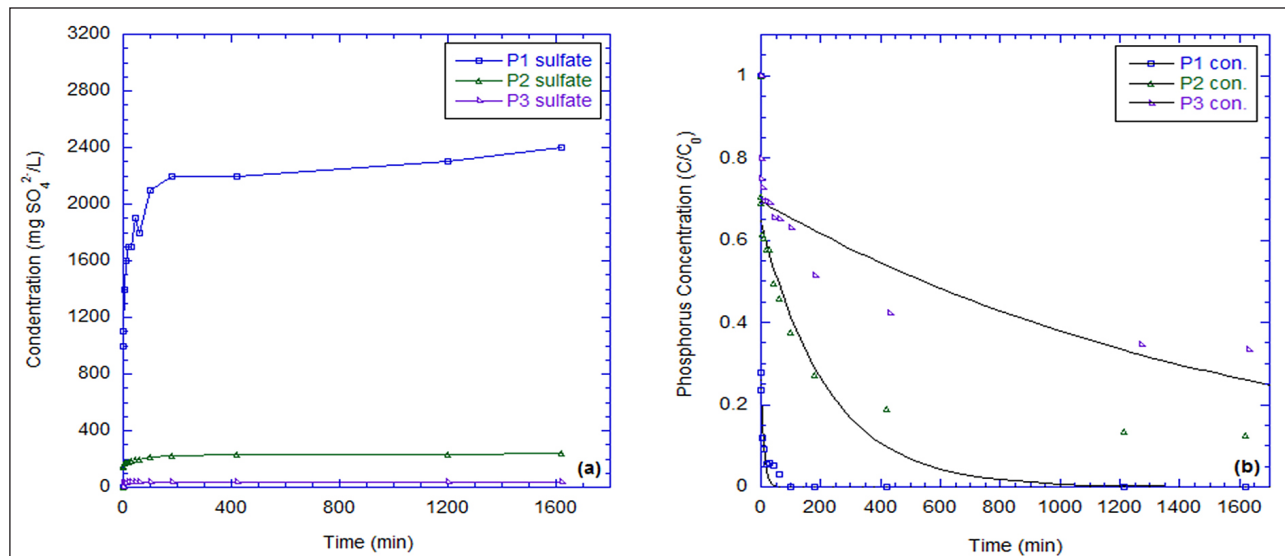
Batch adsorption tests

Linear, Freundlich, and Langmuir models were fitted to the isotherm data using least-squares approximations. Results of batch adsorption tests are shown in Fig. 10 and fitting parameters are summarized in Table 6. As the coefficients of determination of the linear and Freundlich models are $R^2 = 0.685$ and $R^2 = 0.794$, respectively, the Langmuir model is more appropriate as it has the highest coefficient of determination ($R^2 = 0.9919$). The adsorption constant (K_l) for the Langmuir model is 1.403 L·mg^{-1} with a Q_{max} of 8.921 mg·g^{-1}. Q_{max} for phosphorus using various adsorbents are summarized in Table 7. Kanuma mud, geothite, lagoon fly ash, wood fibre, alumina-coated carboxylate, ACF-La, and lanthanum-doped vesuvianite showed lower Q_{max} than that of this study (Saha et al., 2008; Yang et al., 2013; Zhang et al., 2011; Cheung and Venkitachalam, 2000; Zhong et al., 2007; Eberhardt et al., 2006; Li et al., 2009). Other adsorbents showed extremely high Q_{max} for phosphorus, of greater than 100 mg·g^{-1} (Choi et al., 2012; Wen et al., 2014).

Table 8. Instantaneous partition coefficients, first-order rate constants and removal rates of SCV under various conditions

Conditions	Amount of SCV (g)	Final sulfate concentration (mg·L⁻¹)	Initial P concentration (mg·L⁻¹)	%P removal after reaction	K_{obs} (h⁻¹)	K_p (L·kg⁻¹)
Phase 1 (P1)	1.0	2 400	40	99.99	0.361	113.2
Phase 2 (P2)	1.0	240	40	87.5	0.0069	21.8
Phase 3 (P3)	1.0	40	40	66.75	0.00087	17.5

Figure 11. Results of sequential leaching tests for 25 g·L⁻¹ SCV with an initial phosphorus concentration of 40 mg·L⁻¹: (a) leached concentrations of sulfate after first, second, and third

Leaching of sulfate from SCV and effects on phosphorus removal

Sequential batch leaching tests were conducted to determine the amount of sulfate leached from SCV and its effects on phosphate removal. Test results are shown in Fig. 11 and summarized in Table 8.

In the first test (Phase 1, P1), the concentration of sulfate was dramatically increased from 0 to 1 800 mg·L⁻¹ within 60 min and slowly increased to 2 400 mg·L⁻¹. The leached concentrations of sulfate, however, were decreased to 240 mg·L⁻¹ in the second test (Phase 2, P2) and 40 mg·L⁻¹ in the third test (Phase 3, P3).

During the sequential batch leaching tests, phosphate concentrations were measured and analysed using Eq. 4 to obtain the kinetic parameters for phosphate removal. The removal rates of phosphate at a time of 1 600 min were 99.99% (P1), 87.5% (P2), and 66.75% (P3). The removal rate constant (K_{obs}) was rapidly decreased from 0.361 h⁻¹ (P1) to 0.00087 h⁻¹ (P3). Similar results were obtained for the instantaneous partition coefficient (K_p). The K_p (L·kg⁻¹) was quickly decreased from 113.2 at P1 to 17.5 at P3.

In the first test, concentration of sulfate was 2 400 mg·L⁻¹, and in the second sulfate was only 240 mg·L⁻¹. At the same time, phosphate removal efficiency decreased from 99.9 to 87.5%. A larger decrease in phosphate removal efficiency can be expected with decreased sulfate concentration. In the third experiment, as the sulfate concentration decreased from 240 mg·L⁻¹ to 40 mg·L⁻¹, the phosphorus removal efficiency decreased from 87.5% to 66.75%. The change in sulfate concentration is much larger than the change in phosphorus removal efficiency.

Therefore, the removal mechanism for phosphate was assumed to be the anion exchange with sulfate coated on the SCV.

Column tests

Results for the column tests are shown in Fig. 12 and Table 9. The effect of influent phosphate concentration on the breakthrough curve was examined in the range of 10–50 mg·L⁻¹ at a flow rate of 5 mL·min⁻¹. Increasing influent phosphate concentration resulted in decreasing the breakthrough time (Fig. 12a). A decrease in phosphate concentration resulted in a later breakthrough curve, and the treated volume of phosphate solution was greatest at the lowest influent concentration. In addition, the bed adsorption capacity (q_e, mg·g⁻¹) increased from 7.5 to 19.5 at influent phosphate concentration of 10 and 50 mg·L⁻¹, respectively. This could be explained by the high influent phosphate concentration, which provided a greater driving force for the transfer process to overcome mass transfer resistance (Na and Park, 2011; Woumfo et al., 2015); an increased ratio of phosphate to SCV amount also resulted in higher q_e.

Table 9. Column data parameter obtained at different influent phosphate concentration and flow rates

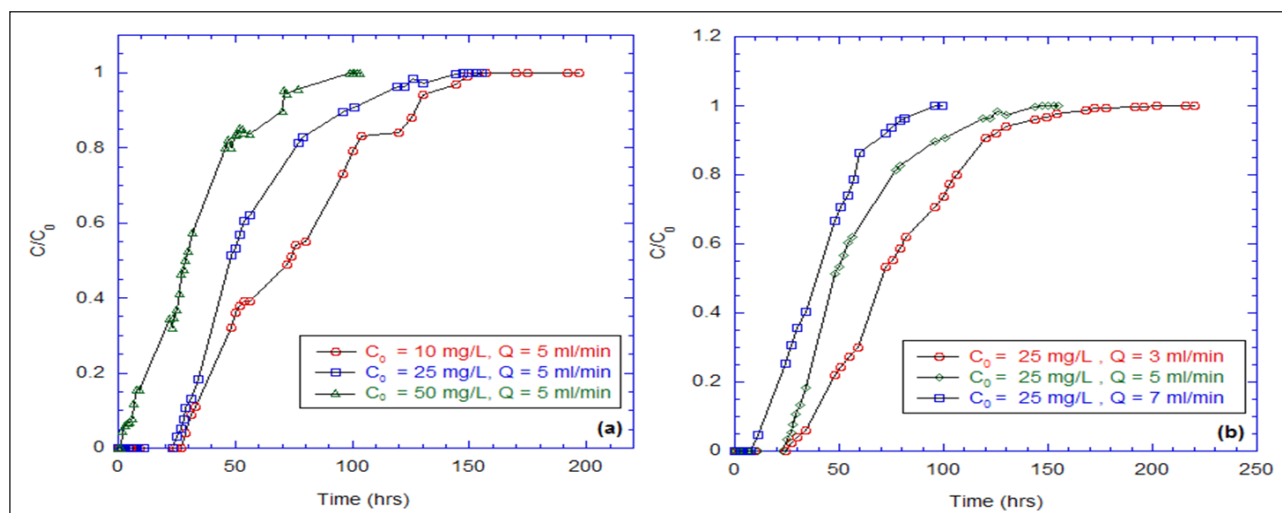| Adsorbent	Exp. parameters	C_0 (mg·L⁻¹)	Q (mL·min⁻¹)	H (cm)	EBCT (min)	q_e (mg·g⁻¹)
SCV	Initial con. (C_0)	10	5	30	142.54	7.47
		25	5	30	142.54	14.69
		50	5	30	142.54	19.53
	Flow rate	25	3	30	237.58	16.63
		25	5	30	142.54	14.69
		25	7	30	101.82	13.14

Figure 12. Results of column sorption tests for SCV at (a) different initial phosphorus concentrations at a fixed flow rate (5 mL·min⁻¹), and (b) different flow rates at a fixed initial phosphorus concentration of 25 mg·L⁻¹

The effect of flow rate on the adsorption of phosphate was tested in the ranges of 3–7 mL·min⁻¹ at an influent phosphate concentration of 25 mg·L⁻¹. Breakthrough occurred faster at an increased flow rate. As the flow rate increased from 3 to 7 mL·min⁻¹, the EBCT decreased from 237.6 to 101.8 min (Table 9), and q_e (mg·g⁻¹) decreased from 16.6 to 13.1 (Table 9). The breakthrough curve became steeper as the flow rate increased because the phosphate did not have enough contact time with SCV at a high flow rate. This low contact time resulted in a lower phosphate removal efficiency.

Sun et al. (2014) reported that the q_e had a range of 11.6–21.1 mg·g⁻¹ in a column test using oxidized Mg_3–Fe, and Woumfo et al. (2015) suggested a range of 2.8–5.9 mg·g⁻¹ using an andosol–bagasse mixture. In the case of silica sulfate, Jutidamrongphan et al. (2012) reported a q_e of 37.6 mg·g⁻¹, higher than the q_e of the present study.

CONCLUSIONS

The following conclusions were obtained after we evaluated the applicability of EV and SCV as adsorbents, and their adsorption capacity for removal of phosphorus from an aqueous solution. In general, EV was not effective for phosphorus removal but SCV showed good removal capacity for phosphorus.

Results of serial batch kinetic tests with SCV showed rapid phosphorus removal rates that could be successfully modelled by a first-order model with instantaneous adsorption. The rate constants and instantaneous partition coefficients increased with SCV/solution ratio. The removal rate constant K_{obs} (h⁻¹) shows a rapidly increasing pattern as the amount of SCV increases: 0.00015 at 1.0 g·L⁻¹ to 0.5002 at 25 g·L⁻¹. Furthermore, the instantaneous partition coefficient K_p (L·kg⁻¹) was quickly increased, similarly to the removal rate constant, from 58.97 at 1 g·L⁻¹ to 166.61 at 25 g·L⁻¹.

For the tests with different initial phosphorus concentrations, the removal rate constants (K_{obs}, h⁻¹) decreased with initial phosphorus concentration but the instantaneous partition coefficients showed similar values regardless of initial phosphorus concentration.

From pseudo first-order and pseudo second-order model fits on the batch kinetic data, we found that the process of phosphate adsorption onto SCV was well described by the pseudo second-order model because of the high determination coefficient.

From the batch adsorption tests, we found that the Langmuir model was the most appropriate. The adsorption constant (K_l) for the Langmuir model was 1.403 L·mg⁻¹ and Q_{max} of 8.921 mg·g⁻¹.

The bed adsorption capacity (q_e) obtained from the column tests at a flow rate of 5 mL·min⁻¹ were 7.47, 14.69 and 19.53 mg·g⁻¹ at initial concentrations of 10, 25 and 50 mg·L⁻¹, respectively.

The adsorption capacity values from the batch adsorption (Q_{max}) and the column tests (q_e) were significantly different. We assume that a better adsorption environment was provided by the column tests rather than the batch adsorption tests.

The SCV used in this study showed excellent adsorption capacity compared to various sorbents evaluated in other studies. In particular, the SCV showed rapid phosphorus removal rates via instantaneous adsorption reaction and also had floating ability. In addition, the floating ability of SCV could give additional potential for the separation of SCV and water.

REFERENCES

AKAY G, KESKINLER B, CAKICI A and DANIS U (1998) Phosphate removal from water by red mud using crossflow microfiltration. *Water Res.* **32** (3) 717–726. https://doi.org/10.1016/S0043-1354(97)00236-4

AWUAL M and JYO A (2011) Assessing of phosphorus removal by polymeric anion exchangers. *Desalination.* **281** (2) 111–117. https://doi.org/10.1016/j.desal.2011.07.047

BISWAS B, INOUE K, GHIMIRE K, OHTA S, HARADA H, OHTO K and KAWAKITA H (2007) The adsorption of phosphate from an aquatic environment using metal-loaded orange waste. *J. Colloid Interf. Sci.* **312** (2) 214–223. https://doi.org/10.1016/j.jcis.2007.03.072

BISWAS B, INOUE K, GHIMIRE K, HARADA H, OHTO K and KAWAKITA H (2008) Removal and recovery of phosphorus from water by means of adsorption onto orange waste gel loaded with zirconium. *J. Bioresour. Technol.* **99** (18) 8685–8690. https://doi.org/10.1016/j.biortech.2008.04.015

BOWDEN L, JARVIS A, YOUNGER P and JOHNSON K (2009) Phosphorus removal from waste waters using basic oxygen steel slag. *Environ. Sci. Technol.* **43** (7) 2476–2481. https://doi.org/10.1021/es801626d

CABRITA M, SILVA A, OLIVEIRA P, ANGÉLICO M and NOGUEIRA M (2015) Assessing eutrophication in the Portuguese continental Exclusive Economic Zone within the European Marine Strategy Framework Directive. *Ecol. Indicators.* **58** (2) 286–299. https://doi.org/10.1016/j.ecolind.2015.05.044

CHEN L, WU P, CHEN M, LAI X, AHMED Z, ZHU N, DANG Z, BI Y and LIU T (2018) Preparation and characterization of the eco-friendly chitosan/vermiculite biocomposite with excellent removal capacity for cadmium and lead. *Appl. Clay Sci.* **159** (1) 74–82. https://doi.org/10.1016/j.clay.2017.12.050

CHEUNG K and VENKITACHALAM T (2000) Improving phosphate removal of sand infiltration system using alkaline fly ash. *Chemosphere*. **41** (1) 243–249. https://doi.org/10.1016/S0045-6535(99)00417-8

CHOI J, LEE S, LEE S, KIM E, PARK K, KIM D and HONG S (2012) Comparison of surface-modified adsorbents for phosphate removal in water. *Water Air Soil Pollut*. **223** (6) 2881–2890. https://doi.org/10.1007/s11270-011-1072-6

CODD G, MORRISON L and METCALF J (2005) Cyanobacterial toxins: risk management for health protection. *Toxicol. Appl. Pharmacol*. **203** (3) 264–272. https://doi.org/10.1016/j.taap.2004.02.016

DE-BASHAN L and BASHAN Y (2004) Recent advances in removing phosphorus from wastewater and its future use as fertilizer (1997–2003). *Water Res*. **38** (19) 4222–4246. https://doi.org/10.1016/j.watres.2004.07.014

DEL CASTILLO H, GIL A and GRANGE P (1997) Preparation and characterization of sulfated titanium-modified pillared montmorillonite. *Catal. Lett*. **43** (1/2) 133–137. https://doi.org/10.1023/A:1018945329164

DITTMANN E and WIEGAND C (2006) Cyanobacterial toxins – occurrence, biosynthesis and impact on human affairs. *Mol. Nutr. Food Res*. **50** (1) 7–17. https://doi.org/10.1002/mnfr.200500162

EBERHARDT T, MIN S and HAN J (2006) Phosphate removal by refined aspen wood fiber treated with carboxymethyl cellulose and ferrous chloride. *Bioresour. Technol*. **97** (18) 2371–2376. https://doi.org/10.1016/j.biortech.2005.10.040

ESTRADA V, MAGGIO J and DIAZ M (2011) Water sustainability: A systems engineering approach to restoration of eutrophic Lakes. *Comp. Chem. Eng*. **35** (8) 1598–1613. https://doi.org/10.1016/j.compchemeng.2011.03.003

GUAN Q, HU X, WU D, SHANG X, YE C and KONG H (2009) Phosphate removal in marine electrolytes by zeolite synthesized from coal fly ash. *Fuel*. **88** (9) 1643–1649. https://doi.org/10.1016/j.fuel.2009.02.031

HUANG W, YU X, TANG J, ZHU Y, ZHANG Y and LI D (2015) Enhanced adsorption of phosphate by flower-like mesoporous silica spheres loaded with lanthanum. *Micropor. Mesopor. Mater*. **217** (2) 225–232. https://doi.org/10.1016/j.micromeso.2015.06.031

JUNG O, CHOI H and CHEONG K (2000) Phosphorus removal from synthetic wastewater by waste oyster shells. *J. Environ. Health Sci*. **26** (1) 43–49 (in Korean).

JUTIDAMRONGPHAN W, PARK K, DOCKKO S, CHOI J and LEE S (2012) High removal of phosphate from wastewater using silica sulfate. *Environ. Chem. Lett*. **10** (1) 21–28. https://doi.org/10.1007/s10311-011-0323-5

KARACA S, GÜRSES A, EJDER M and ACIKYILDIZ M (2004) Kinetic modeling of liquid-phase adsorption of phosphate on dolomite. *J. Colloid Interf. Sci*. **277** (2) 257–263. https://doi.org/10.1016/j.jcis.2004.04.042

KARTASHEVSKY M, SEMIAT R and DOSORETZ C (2015) Phosphate adsorption on granular ferric hydroxide to increase product water recovery in reverse osmosis-desalination of secondary effluents. *Desalination*. **364** (1) 53–61. https://doi.org/10.1016/j.desal.2015.02.038

KIM J, LIM C, KIM K, KIM D, LEE S and KIM J (2008) Application of adsorption characteristic of ferrous iron waste to phosphate removal from municipal wastewater. *J. Kor. Soc. Environ. Agric*. **27** (2) 231–238 (in Korean). https://doi.org/10.5338/KJEA.2008.27.3.231

KIM S and LEE T (2014) A study for the removal of phosphorous using coated exfoliated vermiculite. *J. Kor. Geo-Environ. Soc*. **15** (1) 5–13 (in Korean). https://doi.org/10.14481/jkges.2014.15.12.5

KOPPENSTEINER B (1998) The degradation of the herbicides alachlor and metolachlor by iron metal in water and soil systems. MSc dissertation, University of Wisconsin Madison. 83 pp.

KUMAR P, SUDHA S, CHAND S and SRIVASTAVA V (2010) Phosphate removal from aqueous solution using coir-pith activated carbon. *Sep. Sci. Technol*. **45** (10) 1463–1470. https://doi.org/10.1080/01496395.2010.485604

LAPOINTE B, HERREN L, DEBORTOLI D and VOGEL M (2015) Evidence of sewage-driven eutrophication and harmful algal blooms in Florida's Indian River Lagoon. *Harmful Algae*. **43** (1) 82–102. https://doi.org/10.1016/j.hal.2015.01.004

LEE Y and YIM S (2011) Adsorption removal of phosphate from aqueous solution by olivine. *J. Kor. Soc. Water Qual*. **27** (4) 516–522. (In Korean).

LI H, RU J, YIN W, LIU X, WANG J and ZHANG W (2009) Removal of phosphate from polluted water by lanthanum doped vesuvianite. *J. Hazardous Mater*. **168** (1) 326–330. https://doi.org/10.1016/j.jhazmat.2009.02.025

LIU C, WU P, ZHU Y and TRAN L (2016) Simultaneous adsorption of Cd^{2+} and BPA on amphoteric surfactant activated montmorillonite. *Chemosphere*. **144** (8) 1026–1032. https://doi.org/10.1016/j.chemosphere.2015.09.063

LIU S, WU P, CHEN M, YU L, KANG C, ZHU N and DANG Z (2017) Amphoteric modified vermiculites as adsorbents for enhancing removal of organic pollutants: bisphenol A and tetrabromobisphenol A. *Environ. Pollut*. **228** (2) 277–286. https://doi.org/10.1016/j.envpol.2017.03.082

LONG H, WU P, YANG L, HUANG Z, ZHU N and HU Z (2014) Efficient removal of cesium from aqueous solution with vermiculite of enhanced adsorption property through surface modification by ethylamine. *J. Colloid Interf. Sci*. **428** (2) 295–301. https://doi.org/10.1016/j.jcis.2014.05.001

LU N and LIU J (2010) Removal of phosphate and fluoride from wastewater by a hybrid precipitation–microfiltration process. *Sep. Purif. Technol*. **74** (3) 329–335. https://doi.org/10.1016/j.seppur.2010.06.023

LÜRLING M and OOSTERHOUT F (2013) Controlling eutrophication by combined bloom precipitation and sediment phosphorus inactivation. *Water Res*. **47** (17) 6527–6537. https://doi.org/10.1016/j.watres.2013.08.019

LÜRLING M, WAAJEN G and OOSTERHOUT F (2014) Humic substances interfere with phosphate removal by lanthanum modified clay in controlling eutrophication. *Water Res*. **54** (1) 78–88. https://doi.org/10.1016/j.watres.2014.01.059

MALANDRINO M, ABOLLINO O, GIACOMINO A, ACETO M and MENTASTI E (2006) Adsorption of heavy metals on vermiculite: Influence of pH and organic ligands. *J. Colloid Interf. Sci*. **299** (2) 537–546. https://doi.org/10.1016/j.jcis.2006.03.011

MCBRIDE M (1994) *Environmental Chemistry of Soils*. Oxford University, Oxford.

MEDEIROS M, SANSIVIERO M, ARAÚJO M and LAGO R (2009) Modification of vermiculite by polymerization and carbonization of glycerol to produce highly efficient materials for oil removal. *Appl. Clay Sci*. **45** (4) 213–219. https://doi.org/10.1016/j.clay.2009.06.008

MUIAMBO H, FOCKE W, ATANASOVA M and BENHAMIDA A (2015) Characterization of urea-modified palabora vermiculite. *Appl. Clay Sci*. **105** (1) 14–20. https://doi.org/10.1016/j.clay.2014.12.019

MÜNCH E and BARR K (2001) Controlled struvite crystallisation for removing phosphorus from anaerobic digester sidestreams. *Water Res*. **35** (1) 151–159. https://doi.org/10.1016/S0043-1354(00)00236-0

NA C and PARK H (2011) Applicability of theoretical adsorption models for studies on adsorption properties of adsorbents[II]. *J. Kor. Soc. Environ. Eng*. **33** (4) 804–811. https://doi.org/10.4491/KSEE.2011.33.11.804

NGUYEN T, NGO H, GUO W, LIANG S, LEE D, NGUYEN P and BUI X (2014) Modification of agricultural waste/by-products for enhanced phosphate removal and recovery: Potential and obstacles. *Bioresour. Technol*. **169** (3) 750–762. https://doi.org/10.1016/j.biortech.2014.07.047

NING P, BART H, LI B, LU X and ZHANG Y (2008) Phosphate removal from wastewater by model-La(III) zeolite adsorbents. *J. Environ. Sci*. **20** (6) 670–674. https://doi.org/10.1016/S1001-0742(08)62111-7

OGATA F, IMAI D, TODA M, OTANI M and KAWASAKI N (2015) Adsorption of phosphate ion in aqueous solutions by calcined cobalt hydroxide at different temperatures. *J. Environ. Chem. Eng*. **3** (3) 1570–1577. https://doi.org/10.1016/j.jece.2015.05.028

OLADOJA N, OLOLADE I, ADESINA A, ADELAGUN R and SANI Y (2013) Appraisal of gastropod shell as calcium ion source for phosphate removal and recovery in calcium phosphate minerals crystallization procedure. *Chem. Eng. Res. Design*. **91** (5) 810–818. https://doi.org/10.1016/j.cherd.2012.09.017

PELEKA E and DELIYANNI E (2009) Adsorptive removal of phosphates from aqueous solutions. *Desalination*. **245** (1) 357–371. https://doi.org/10.1016/j.desal.2008.04.050

PRADHAN J, DAS J, DAS S and THAKUR R (1998) Adsorption of phosphate from aqueous solution using activated red mud. *J. Colloid Interf. Sci*. **204** (1) 169–172. https://doi.org/10.1006/jcis.1998.5594

RUIXIA L, JINLONG G and HONGXIAO T (2002) Adsorption of fluoride, phosphate, and arsenate ions on a new type of ion exchange fiber. *J. Colloid Interf. Sci.* **248** (2) 268–274. https://doi.org/10.1006/jcis.2002.8260

SAHA B, CHAKRABORTY S and DAS G (2008) A mechanistic insight into enhanced and selective phosphate adsorption on a coated carboxylated surface. *J. Colloid Interf. Sci.* **331** (1) 21–26. https://doi.org/10.1016/j.jcis.2008.11.007

SHIN E, HAN J, JANG M, MIN S, PARK J and ROWELL R (2004) Phosphate adsorption on aluminium-impregnated mesoporous silicates: surface structure and behavior of adsorbents. *Environ. Sci. Technol.* **38** (3) 912–917. https://doi.org/10.1021/es030488e

SONG J, LEE J, KIM S and LEE T (2009) Evaluation of removal properties of Cu(Ⅱ) from aqueous solutions by inflated vermiculites. *J. Kor. Geo-Environ. Soc.* **10** (1) 25–32 (in Korean).

SONG Y, YUAN P, ZHENG B, PENG J, YUAN F and GAO Y (2007) Nutrients removal and recovery by crystallization of magnesium ammonium phosphate from synthetic swine wastewater. *Chemosphere.* **69** (2) 319–324. https://doi.org/10.1016/j.chemosphere.2007.06.001

SOUSA A, BRAGA T, GOMES E, VALENTINI A and LONGHINOTTI E (2012) Adsorption of phosphate using mesoporous spheres containing iron and aluminum oxide. *J. Chem. Eng.* **210** (1) 143–149. https://doi.org/10.1016/j.cej.2012.08.080

SUN X, IMAI T, SEKINE M, HIGUCHI T, YAMAMOTO K, KANNO A and NAKAZONO S (2014) Adsorption of phosphate using calcined Mg3-Fe layered double hydroxides in a fixed-bed column study. *J. Ind. Eng. Chem.* **20** (5) 3623–3630. https://doi.org/10.1016/j.jiec.2013.12.057

TEKILE A, KIM I and KIM J (2015) Mini-review on river eutrophication and bottom improvement techniques, with special emphasis on the Nakdong River. *J. Environ. Sci.* **30** (1) 113–121. https://doi.org/10.1016/j.jes.2014.10.014

UNNITHAN M, VINOD V and ANIRUDHAN T (2002) Ability of Iron(III)-Loaded carboxylated polyacrylamide-grafted sawdust to remove phosphate ions from aqueous solution and fertilizer industry wastewater: Adsorption kinetics and isotherm studies. *J. Appl. Polymer Sci.* **84** (13) 2541–2553. https://doi.org/10.1002/app.10579

VAIOPOULOU E, MELIDIS P and AIVASIDIS A (2007) Growth of filamentous bacteria in an enhanced biological phosphorus removal system. *Desalination.* **213** (1) 288–296. https://doi.org/10.1016/j.desal.2006.02.101

WEN Z, ZHANG Y and DAI C (2014) Removal of phosphate from aqueous solution using nanoscale zerovalent iron (nZVI). *Colloids and Surfaces A. Physicochem. Eng. Aspects.* **457** (3) 433–440. https://doi.org/10.1016/j.colsurfa.2014.06.017

WOUMFO E, SIEWE J and NJOPWOUO D (2015) A fixed-bed column for phosphate removal from aqueous solutions using an andosol-bagasse mixture. *J. Environ. Manage.* **151** (2) 450–460. https://doi.org/10.1016/j.jenvman.2014.11.029

YANG S, DING D, ZHAO Y, HUANG W, ZHANG Z, LEI Z and YANG Y (2013) Investigation of phosphate adsorption from aqueous solution using Kanuma mud: Behaviors and mechanisms. *J. Environ. Chem. Eng.* **1** (3) 355–362. https://doi.org/10.1016/j.jece.2013.05.016

YANG S, WU P, LIU J, CHEN M, AHMED Z and ZHU N (2018) Efficient removal of bisphenol A by superoxide radical and singlet oxygen generated from peroxymonosulfate activated with Fe^0-montmorillonite. *Chem. Eng. J.* **350** (3) 484–495. https://doi.org/10.1016/j.cej.2018.04.175

YEOM S and JUNG K (2008) Recycling wasted scallop shell as an adsorbent for the removal of phosphate. *J. Ind. Eng. Chem.* **15** (1) 40–44. https://doi.org/10.1016/j.jiec.2008.08.014

YUAN M, CARMICHAEL W and HILBORN E (2006) Microcystin analysis in human sera and liver from human fatalities in Caruaru, Brazil 1996. *Toxicon.* **48** (6) 627–640. https://doi.org/10.1016/j.toxicon.2006.07.031

YU X, WEI C, KE L, HU Y, XIE X and WU H (2010) Development of organovermiculite-based adsorbent for removing anionic dye from aqueous solution. *J. Hazardous Mater.* **180** (1) 499–507. https://doi.org/10.1016/j.jhazmat.2010.04.059

ZENG L, LI X and LIU J (2004) Adsorptive removal of phosphate from aqueous solutions using iron oxide tailings. *Water Res.* **38** (5) 1318–1326. https://doi.org/10.1016/j.watres.2003.12.009

ZHANG L, WAN L, CHANG N, LIU J, DUAN C, ZHOU Q, LI X and WANG X (2011) Removal of phosphate from water by activated carbon fiber loaded with lanthanum oxide. *J. Hazardous Mater.* **190** (1) 848–855. https://doi.org/10.1016/j.jhazmat.2011.04.021

ZHONG B, STANFORTH R, WU S and CHEN J (2007) Proton interaction in phosphate adsorption onto goethite. *J. Colloid Interf. Sci.* **308** (1) 40–48. https://doi.org/10.1016/j.jcis.2006.12.055